

# $^1\text{H}$ , $^{13}\text{C}$ and $^{15}\text{N}$ resonance assignments of the RodA hydrophobin from the opportunistic pathogen *Aspergillus fumigatus*

Ariane Pille · Ann H. Kwan · Ivan Cheung · Matthew Hampsey · Vishukumar Aimaniananda · Muriel Delepierre · Jean-Paul Latgé · Margaret Sunde · J. Iñaki Guijarro

Received: 12 February 2014 / Accepted: 15 March 2014 / Published online: 22 March 2014  
© Springer Science+Business Media Dordrecht 2014

**Abstract** Hydrophobins are fungal proteins characterised by their amphipathic properties and an idiosyncratic pattern of eight cysteine residues involved in four disulphide bridges. The soluble form of these proteins spontaneously self-assembles at hydrophobic/hydrophilic interfaces to form an amphipathic monolayer. The RodA hydrophobin of the opportunistic pathogen *Aspergillus fumigatus* forms an amyloid layer with a rodlet morphology that covers the surface of fungal spores. This rodlet layer bestows hydrophobicity to the spores facilitating their dispersal in the air and rendering the conidia inert relative to the human

immune system. As a first step in the analysis of the solution structure and self-association of RodA, we report the  $^1\text{H}$ ,  $^{13}\text{C}$  and  $^{15}\text{N}$  resonance assignments of the soluble monomeric form of RodA.

**Keywords** Hydrophobin · Functional amyloids · Rodlets · Cell wall · *Aspergillus fumigatus* · NMR

## Biological context

Hydrophobins are small (<20 kDa) amphipathic proteins produced by most filamentous fungi. These proteins with remarkable physicochemical properties are defined by a pattern of eight cysteine (Cys) residues that form four disulphide bonds (C1–C6, C2–C5, C3–C4, C7–C8) (Kwan et al. 2006). They are produced in a soluble form that spontaneously self-assembles at hydrophobic/hydrophilic or air/water interfaces to form amphipathic monolayers with high surfactant activity. Hydrophobins are divided in two classes based on their sequence, hydrophathy and on the physicochemical characteristics of the monolayers (Wosten et al. 1994). Class I hydrophobins show very little conservation in their amino acid sequence and vary in size, with different spacings between cysteine residues; these hydrophobins associate into very robust monolayers that are resistant to detergents even at boiling temperatures and require concentrated acids to dissociate. Class I hydrophobin monolayers show a very well ordered rodlet morphology and display the hallmarks of amyloid fibres (Wosten and de Vocht 2000). The amino acid sequences of class II hydrophobins are more conserved, they show less size and inter-cysteine-spacing variability; the corresponding monolayers do not contain amyloid fibres and can be disaggregated with detergents and hot alcohol solutions.

A. Pille · M. Delepierre · J. I. Guijarro (✉)  
Unité de RMN des Biomolécules, Dépt. Biologie Structurale et Chimie, Institut Pasteur, 25 rue Du Dr. Roux, 75015 Paris, France  
e-mail: inaki.guijarro@pasteur.fr

A. Pille · M. Delepierre · J. I. Guijarro  
CNRS UMR 3528, 75015 Paris, France

A. Pille  
Sorbonne Universités, UPMC Univ Paris 06, IFD,  
4 Place Jussieu, 75252 Paris Cedex 05, France

A. H. Kwan · I. Cheung · M. Hampsey  
School of Molecular Bioscience, University of Sydney, Sydney, NSW 2006, Australia

V. Aimaniananda · J.-P. Latgé  
Unité des *Aspergillus*, Dépt de Parasitologie et Mycologie, Institut Pasteur, 28 rue Du Dr. Roux, 75015 Paris, France

M. Sunde  
School of Medical Sciences, University of Sydney, Sydney, NSW 2006, Australia

Although some degree of order has been observed for hydrophobins HFBI (Szilvay et al. 2007) and NC2 monolayers (Ren et al. 2013a), class II hydrophobins seem to form less well ordered monolayers. The structures of the soluble forms of hydrophobins from both classes that self-associate into monolayers are quite different but show a common central  $\beta$ -barrel stabilised by the four disulphide bridges and surrounding loops of different length and secondary structure (Sunde et al. 2008). The biological functions of hydrophobins rely on the formation of the amphipathic monolayers. Hydrophobins are used by fungi to breach the air/water barrier and develop aerial hyphae by lowering the surface tension of the aqueous environment, to prevent water-logging, to facilitate aerial growth and spore dispersion, to participate in the extracellular matrix and biofilms as well as to form a protective layer during fruiting body development. Hydrophobins can also participate in host-fungi interactions and have been described as pathogenicity factors in plant- or entomo-pathogenic fungi. The surfactant activity of hydrophobins and the capacity to reverse the wettability of surfaces offers the possibility to use these proteins for different biotechnological applications such as drug delivery, cell attachment, surface functional modification and protein purification. The biological functions, structural knowledge and biotechnical applications of hydrophobins have been reviewed in (Wosten 2001; Scholtmeijer et al. 2001; Tucker and Talbot 2001; Linder et al. 2005; Bayry et al. 2012; Ren et al. 2013b).

*Aspergillus fumigatus* is an opportunistic pathogen than can cause a variety of diseases in immunocompromised individuals that range from allergies to threatful invasive aspergillosis. This filamentous fungus has become the major aerial fungal pathogen of humans and represents a major burden in terms of morbidity, mortality and cost for hospitals (Hayes and Denning 2013). The conidia, which are the infective form of the fungus, are covered by a rodlet layer formed by the class I hydrophobin RodA (Paris et al. 2003). This proteinaceous coat bestows hydrophobicity to the spores facilitating their dispersal in the air and masks pathogen-associated molecular patterns (PAMPs) thus rendering the conidia inert relative to the innate and adaptive immune systems (Aimanianda et al. 2009). With the aim of understanding the mechanism of rodlet formation and the rodlet structure, as well as shedding light on the possible links between the structure of RodA and its immunologic characteristics, we are analysing the solution structure of RodA, its self-assembly, the structure of the rodlets and the immunological characteristics of RodA mutants. Here we describe the  $^1\text{H}$ ,  $^{15}\text{N}$ ,  $^{13}\text{C}$  resonance assignments of the soluble form of RodA and the comparison of its secondary structure and dynamics with that of other hydrophobins.

## Materials and methods

### Protein preparation

The RodA gene sequence (AAB07707) was cloned into a pHUE expression vector used for other hydrophobins (Kwan et al. 2006) to generate the plasmid pHUE-RodA. The resulting plasmid encodes for a fusion protein ( $\text{H}_6\text{-Ub-RodA}$ ) of N-terminal hexa-histidine-tagged ubiquitin ( $\text{H}_6\text{-Ub}$ ) coupled to RodA and contains a deubiquinating UBP41 enzyme cleavage site between the ubiquitin and RodA proteins. The plasmid also codes for ampicillin resistance.

The protein  $\text{H}_6\text{-Ub-RodA}$  was expressed using the *Escherichia coli* BL21 (DE3) strain. Bacteria were grown at 37 °C in minimal M9 media supplemented with 0.43 g/L of yeast extract without amino acids and without ammonium sulphate (DIFCO), and containing  $^{15}\text{NH}_4\text{Cl}$  (0.52 g/L,  $\geq 98\%$ ) and  $^{13}\text{C}_6$  glucose (2 g/L,  $\geq 98\%$ ) as sole sources of nitrogen and carbon, respectively. When cultures reached an absorbance of 0.6 at 600 nm, expression was induced with 0.5 mM isopropyl- $\beta$ -thio-galactopyranoside. Cells were harvested by centrifugation at 6700 g and 4 °C after 3 h of induction, resuspended in 150 mM Tris-HCl, 300 mM NaCl pH 8, re-pelleted by centrifugation and frozen at -80 °C.

The fusion protein was obtained simultaneously from both the soluble and insoluble fractions under denaturing and reducing conditions, purified by affinity chromatography and folded under oxidative conditions. To extract the protein, the cell pellet was thawed and solubilised with buffer A (10 mM TrisHCl, 100 mM  $\text{NaH}_2\text{PO}_4$ , 4 mM  $\beta$ -mercaptoethanol [ $\beta\text{ME}$ ], 8 M urea pH 8). After eliminating the cell debris by centrifugation,  $\text{H}_6\text{-Ub-RodA}$  was loaded into a nickel column (Hitrap<sup>TM</sup>, GE Healthcare) pre-equilibrated with buffer A. The column was successively washed with the equilibrating buffer prepared at pH 8 and at pH 6.3. The fusion protein was then eluted with the same buffer prepared at pH 4.3. Oxidative refolding was performed by dialysis of the eluted protein at 4 °C against the refolding buffer (50 mM sodium acetate, 100 mM NaCl, pH 5) supplemented with a redox glutathione couple (10 mM reduced, 1 mM oxidised).

RodA was obtained from the fusion protein by cleavage with UBP41 and further purification by affinity chromatography and reverse-phase high-pressure liquid chromatography (HPLC). After the refolding step, the  $\text{H}_6\text{-Ub-RodA}$  containing samples were dialysed against the cleavage buffer (50 mM TrisHCl, 50 mM NaCl, 2 mM  $\text{CaCl}_2$ , pH 8) and incubated at 37 °C for 2.5 h in the presence of the deubiquinating enzyme UBP41 (20:1 w:w protein:protease ratio). The UBP41 protease, which contains a hexa-histidine tag and cleaves at a specific C-terminal site on ubiquitin fusions, was previously prepared as described in (Kwan et al. 2006).  $\text{H}_6$ -ubiquitin, uncleaved

H<sub>6</sub>-Ub-RodA and the histidine-tagged UBP41 protease were removed by affinity chromatography on a nickel Hi-Trap<sup>TM</sup> column. The column was pre-equilibrated with 50 mM TrisHCl, 300 mM NaCl, 2 mM CaCl<sub>2</sub>, 20 mM imidazole, pH 8. The cleaved mixture was loaded on the column after adjusting the NaCl and imidazole concentrations to 300 and 20 mM, respectively. RodA was eluted with the equilibrating buffer. A final HPLC purification step using a semi-preparative reverse phase C18 column (PepRPC 15  $\mu\text{m}$  HR 10/10, Amersham Biosciences) was performed to separate the folded from the unfolded/partially folded forms of RodA, as well as to further purify the protein. The HPLC column was equilibrated with 10 % methanol, 0.1 % TFA. After adjusting the pH to ca. 4 with HCl, the RodA sample was loaded on the column and a linear gradient from 0 to 100 % of acetonitrile (90 min) in equilibrating buffer was applied. Folded RodA-containing samples were pooled and lyophilised. Protein concentrations were determined by the bicinchoninic acid assay (BCA, Pierce Thermo Scientific) and/or absorption spectrophotometry, protein identity and integrity were monitored by SELDI-TOF (surface enhanced laser desorption/ionization time-of-flight) mass spectrometry and N-terminal microsequencing (Protein Analysis and Microsequencing Facility, Institut Pasteur), and purity was assessed by sodium-dodecyl-sulphate polyacrylamide gel electrophoresis under reducing conditions and NMR ( $^{15}\text{N}$ - $^1\text{H}$  HSQC spectra). In addition,  $^{15}\text{N}$ - $^1\text{H}$  HSQC spectra served to establish the foldedness of the HPLC eluted fractions.

The recombinant protein obtained in this way consists of residues 19–159 of RodA and an additional N-terminal Ser residue that remains after cleavage of the fusion. The 18 N-terminal residues coded by the *RodA* gene, which correspond to the secretion signal and are expected to be cleaved by *A. fumigatus* upon secretion, were not cloned.

Doubly labelled RodA was also extracted by acid treatment from *A. fumigatus* spores obtained from minimal media containing  $^{15}\text{N}$  NH<sub>4</sub>Cl and  $^{13}\text{C}_6$  glucose as described (Aimanianda et al. 2009) and purified by reverse-phase C18 HPLC as for the recombinant protein.

### NMR spectroscopy

Doubly labelled ( $^{15}\text{N}$ ,  $^{13}\text{C}$ ) recombinant RodA samples were prepared from lyophilised protein in 20 mM deuterated sodium acetate (CD<sub>3</sub>COONa) buffer pH 4.3, 10 % D<sub>2</sub>O at a protein concentration of 0.36 mM.

NMR experiments were recorded on an Agilent DirectDrive 600 spectrometer (Agilent Technologies, Santa Clara) with a proton resonating frequency of 599.4 MHz. The spectrometer was equipped with a triple resonance cryogenic probe. Experiments were run at 25 °C and referenced to internal sodium 4,4-dimethyl-4-silapentane-1-

sulphonate following IUPAC recommendations. Data were collected using VnmrJ 3.2A (Agilent Technologies), processed with NMRPipe (Delaglio et al. 1995) and analysed with CCPNMR Analysis (Vranken et al. 2005).

Standard two- and three-dimensional experiments were recorded to assign chemical shifts to the protein  $^1\text{H}$ ,  $^{13}\text{C}$  and  $^{15}\text{N}$  nuclei. Backbone and CB resonances were assigned using [ $^1\text{H}$ - $^{13}\text{C}/^{15}\text{N}$ ] HSQC, HNCO, HNCACB, CBCA(CO)NH, HNCA and HNHA spectra. Side chains signals were assigned through H(CC-TOCSY)NNH, C(CC-TOCSY)NNH, HCCH-TOCSY, (HB)CB(CGCD)HD and (HB)CB(CGCDCE)HE experiments.

Typical spectral widths were 12.6 ppm for  $^1\text{H}$ , 31.5 ppm for  $^{15}\text{N}$  and 80 (aliphatic carbon), 14 (carbonyl), 30 (aromatic carbon), 36 ( $\alpha$  carbon), or 22 ppm ( $\beta$  carbon) for  $^{13}\text{C}$  spectral regions.

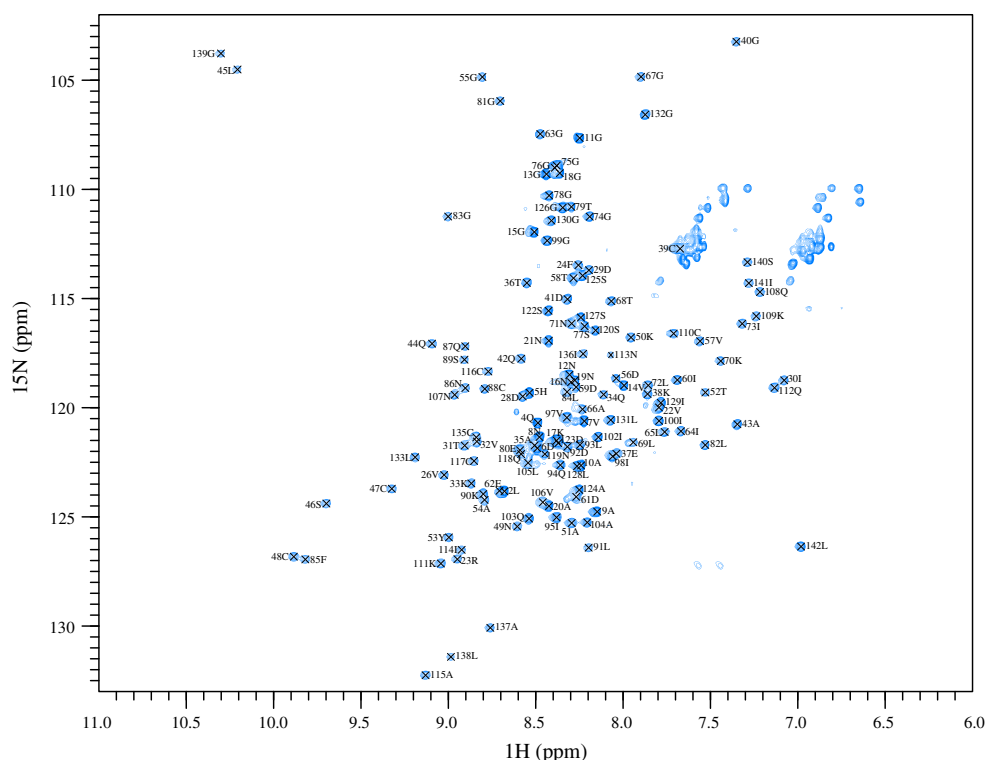
### Assignments and secondary structure

Doubly labelled ( $^{15}\text{N}$ ,  $^{13}\text{C}$ ) recombinant RodA was produced in *E. coli* as a fusion protein with His<sub>6</sub>-tagged ubiquitin. The fusion protein was purified under denaturing conditions, refolded in vitro with a glutathione redox couple, cleaved and further purified by affinity chromatography and reverse-phase HPLC.  $^1\text{H}$ - $^{15}\text{N}$  HSQC spectra (Fig. 1) showed a chemical shift dispersion typical of folded proteins.

The  $^1\text{H}$ ,  $^{13}\text{C}$  and  $^{15}\text{N}$  resonances of RodA were identified following a standard strategy (see Methods) that led to nearly complete assignments. Only side chain exchangeable groups from 4 Asn residues, 8 Lys and one Arg residue, some non-exchangeable side chain resonances (K33 C $\delta$ , K111 C $\epsilon$ He<sub>2</sub>, F23 C $\delta$ , F85 C $\epsilon$  and C $\zeta$ H $\zeta$ ) as well as 8 backbone carbonyls from residues preceding Pro residues and from the C-terminal residue, were not identified. All assigned chemical shifts have been deposited to the BMRB (accession code: 19782).

The redox state of the eight Cys residues of recombinant RodA was analysed using the Cys C $\beta$  and C $\alpha$  chemical shifts as described by Sharma and co-workers (Sharma and Rajarathnam 2000). The data is consistent with all the Cys residues being involved in disulphide bonds. Importantly, preliminary analysis of the pattern of  $^1\text{H}$ - $^1\text{H}$  nuclear Overhauser effects (nOes) observed in  $^{13}\text{C}$  and  $^{15}\text{N}$  edited NOESY spectra (not shown), unambiguously indicated that the disulphide bonds are formed by cysteines C1–C6 (39–116), C2–C5 (47–110), C3–C4 (48–88) and C7–C8 (117–135). The latter pattern is in accordance with the one established by chemical methods for other hydrophobins isolated from fungal sources (Kwan et al. 2006) or by X-ray crystallography from recombinant proteins (Hakanpää et al. 2006a, b), supporting that this pairing is a

**Fig. 1**  $^1\text{H}$ – $^{15}\text{N}$  HSQC spectrum of RodA. The spectrum was recorded at 25 °C in buffer CD<sub>3</sub>COONa 20 mM, 10 % D<sub>2</sub>O, pH 4.3. Assignments are shown only for backbone amide correlations. Chemical shifts ( $\delta$ ) are expressed in ppm relative to DSS (sodium 4,4-dimethyl-4-silapentane-1-sulphonate)



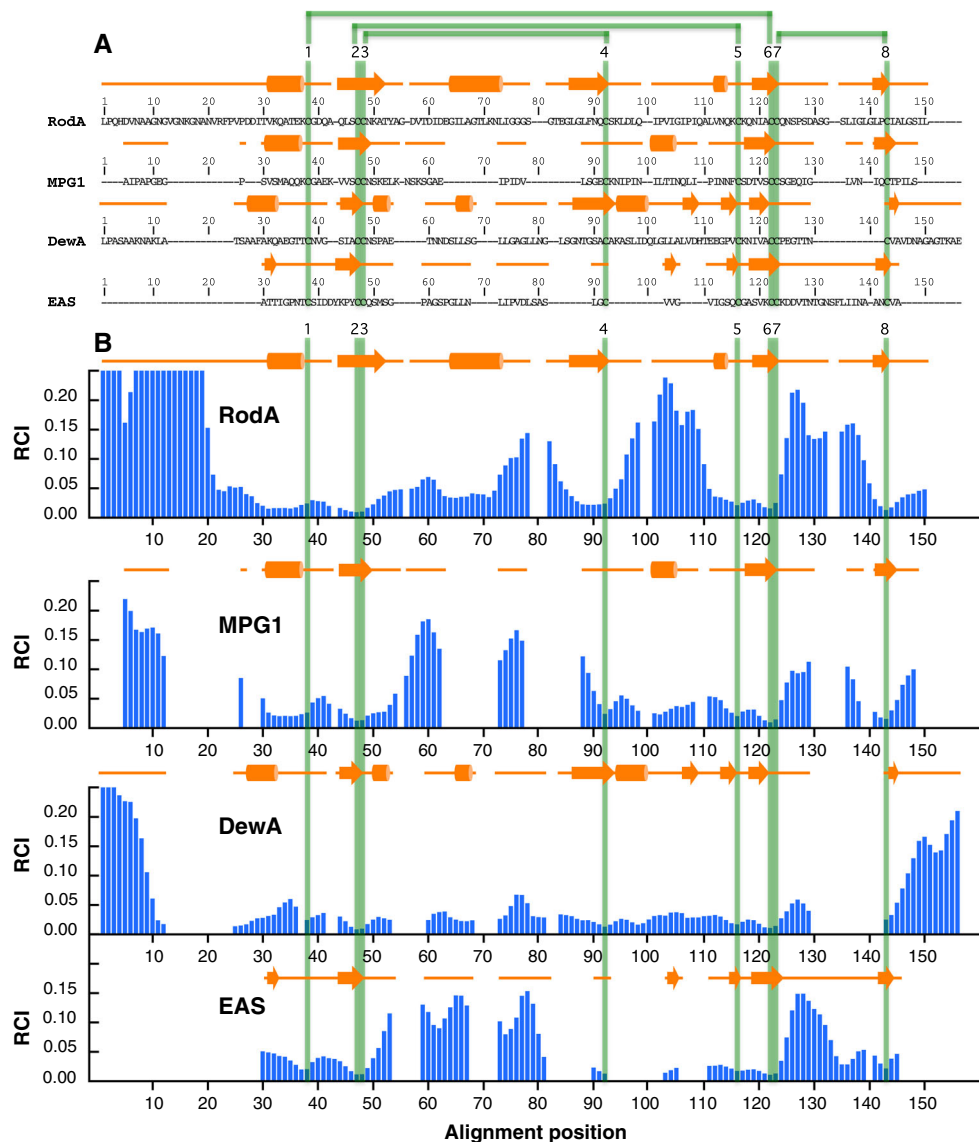


**Fig. 2** **a** Sequence and secondary structure alignment of class I hydrophobins. Sequence alignment of class I hydrophobins with known structure and/or published chemical shifts was obtained by manual modification of a ClustalW alignment (Thompson et al. 1994) with constrained cysteine residue positions. Secondary structure was determined from backbone (N, C, C $\alpha$ , H $\alpha$ ) and C $\beta$  chemical shifts using the PECAN software (RodA and MPG1) or from structural ensembles (DewA and EAS) by means of the DSSP algorithm.  $\alpha$ -helices are represented by cylinders and  $\beta$ -strands by arrows. Positions of Cys residues are numbered from 1 to 8 and are highlighted by horizontal green lines, while the disulphide topology is

regions, differs in the four proteins. In these regions, RodA shows two secondary structure elements that are not observed in EAS, DewA or MPG1: a long  $\alpha$ -helix in the C3–C4 loop and a short  $\alpha$ -helix in the C4–C5 loop. Regarding the nanosecond to picosecond dynamics, the RCI data indicates that the  $\beta$ -barrel region is rather rigid for the four proteins, while the C7–C8 and C3–C4 regions are flexible at least in some segment(s), except for DewA. The C4–C5 region of

indicated by horizontal green lines. **b** Random coil index (RCI) as a function of alignment position. RCI values were calculated from chemical shifts deposited at the BMRB or in the case of EAS with unpublished chemical shifts, using the RCI software (Berjanskii and Wishart 2005). The RCI of the N-terminal residues of RodA and MPG1 are truncated for visualisation purposes. Secondary structure and Cys positions are displayed as in **a**. In **b**, blank spaces represent gap positions in the sequence alignment. Alignment position for RodA starts at residue 2, i.e., at the first residue belonging to RodA in the recombinant protein used in this work

RodA also shows significant dynamics, a feature not observed in the corresponding region in other hydrophobins.

In summary, our data strongly suggest that RodA adopts the characteristic  $\beta$ -barrel topology observed in other hydrophobin structures, and indicates that it displays novel secondary structure elements, as well as a highly flexible N-terminal region and C4–C5 and C7–C8 loops. Interestingly, the highly flexible C7–C8 loop of EAS contains an



amyloidogenic sequence (FLIIN) that has been shown by mutagenesis and peptide experiments to be implicated in the core cross  $\beta$ -structure of the EAS amyloid fibres (Macindoe et al. 2012). Flexibility of regions containing amyloidogenic sequences seems to be an important factor to allow the conformational changes that take place at the interface between hydrophobic and hydrophilic interfaces to form rodlets (Morris et al. 2011). Amyloid prediction algorithms such as AMYLPRED (<http://aias.biol.uoa.gr/AMYLPRED>) predict an amyloidogenic sequence in the C7–C8 loop of RodA (data not shown). The assignments presented in this work open the way for determining the structure of the soluble monomeric form of RodA, which will be valuable for the characterisation of the association mechanism into rodlets and for the study of RodA rodlets, which render the spores of the fungal pathogen *A. fumigatus* inert to the human immune system.

**Acknowledgments** This work was funded by the ANR-10-Blanc SVSE 3-009 HYDROPHOBIN project, the European Community's Seventh Framework Programme [FP7/2007-2013] under Grant Agreement No: 260338 ALLFUN and the French-Australian Science and Technology (FAST) Program 2011. The 600 MHz spectrometer was funded by the Région Ile de France and the Institut Pasteur. We thank Jacques D'Alayer (Institut Pasteur) for initial SELDI-TOF and for N-terminal sequencing experiments.

## References

- Aimanianda V, Bayry J, Bozza S, Kniemeyer O, Perruccio K, Elluru SR, Clavaud C, Paris S, Brakhage AA, Kaveri SV et al (2009) Surface hydrophobin prevents immune recognition of airborne fungal spores. *Nature* 460:1117–1121
- Bayry J, Aimanianda V, Guijarro JJ, Sunde M, Latge JP (2012) Hydrophobins—unique fungal proteins. *PLoS Pathog* 8:e1002700
- Berjanskii MV, Wishart DS (2005) A simple method to predict protein flexibility using secondary chemical shifts. *J Am Chem Soc* 127:14970–14971
- Delaglio F, Grzesiek S, Vuister GW, Zhu G, Pfeifer J, Bax A (1995) NMRPipe: a multidimensional spectral processing system based on UNIX pipes. *J Biomol NMR* 6:277–293
- Eghbalnia HR, Wang L, Bahrami A, Assadi A, Markley JL (2005) Protein energetic conformational analysis from NMR chemical shifts (PECAN) and its use in determining secondary structural elements. *J Biomol NMR* 32:71–81
- Hakanpää J, Linder M, Popov A, Schmidt A, Rouvinen J (2006a) Hydrophobin HFBII in detail: ultrahigh-resolution structure at 0.75 Å. *Acta Crystallogr D Biol Crystallogr* 62:356–367
- Hakanpää J, Szilvay GR, Kaljunen H, Maksimainen M, Linder M, Rouvinen J (2006b) Two crystal structures of *Trichoderma reesei* hydrophobin HFBII—the structure of a protein amphiphile with and without detergent interaction. *Protein Sci* 15:2129–2140
- Hayes GE, Denning DW (2013) Frequency, diagnosis and management of fungal respiratory infections. *Curr Opin Pulm Med* 19:259–265
- Kwan AH, Winefield RD, Sunde M, Matthews JM, Haverkamp RG, Templeton MD, Mackay JP (2006) Structural basis for rodlet assembly in fungal hydrophobins. *Proc Natl Acad Sci USA* 103:3621–3626
- Linder MB, Szilvay GR, Nakari-Setälä T, Penttilä ME (2005) Hydrophobins: the protein-amphiphiles of filamentous fungi. *FEMS Microbiol Rev* 29:877–896
- Macindoe I, Kwan AH, Ren Q, Morris VK, Yang W, Mackay JP, Sunde M (2012) Self-assembly of functional, amphipathic amyloid monolayers by the fungal hydrophobin EAS. *Proc Natl Acad Sci USA* 109:E804–811
- Morris VK, Ren Q, Macindoe I, Kwan AH, Byrne N, Sunde M (2011) Recruitment of class I hydrophobins to the air:water interface initiates a multi-step process of functional amyloid formation. *J Biol Chem* 286:15955–15963
- Morris VK, Kwan AH, Mackay JP, Sunde M (2012) Backbone and sidechain (1)H, (13)C and (15)N chemical shift assignments of the hydrophobin DewA from *Aspergillus nidulans*. *Biomol NMR Assign* 6:83–86
- Morris VK, Kwan AH, Sunde M (2013) Analysis of the structure and conformational states of DewA gives insight into the assembly of the fungal hydrophobins. *J Mol Biol* 425:244–256
- Paris S, Debeaupuis JP, Crameri R, Carey M, Charles F, Prevost MC, Schmitt C, Philippe B, Latge JP (2003) Conidial hydrophobins of *Aspergillus fumigatus*. *Appl Environ Microbiol* 69:1581–1588
- Ren Q, Kwan AH, Sunde M (2013a) Solution structure and interface-driven self-assembly of NC2, a new member of the Class II hydrophobin proteins. *Proteins*. doi:10.1002/prot.24473
- Ren Q, Kwan AH, Sunde M (2013b) Two forms and two faces, multiple states and multiple uses: properties and applications of the self-assembling fungal hydrophobins. *Biopolymers* 100:601–612
- Rey AA, Hoche A, Kwan AH, Sunde M (2013) Backbone and sidechain (1)H, (13)C and (15)N chemical shift assignments of the hydrophobin MPG1 from the rice blast fungus *Magnaporthe oryzae*. *Biomol NMR Assign* 7:109–112
- Scholtmeijer K, Wessels JG, Wosten HA (2001) Fungal hydrophobins in medical and technical applications. *Appl Microbiol Biotechnol* 56:1–8
- Sharma D, Rajarathnam K (2000) <sup>13</sup>C NMR chemical shifts can predict disulfide bond formation. *J Biomol NMR* 18:165–171
- Sunde M, Kwan AH, Templeton MD, Beever RE, Mackay JP (2008) Structural analysis of hydrophobins. *Micron* 39:773–784
- Szilvay GR, Paananen A, Laurikainen K, Vuorimaa E, Lemmetyinen H, Peltonen J, Linder MB (2007) Self-assembled hydrophobin protein films at the air-water interface: structural analysis and molecular engineering. *Biochemistry* 46:2345–2354
- Thompson JD, Higgins DG, Gibson TJ (1994) CLUSTAL W: improving the sensitivity of progressive multiple sequence alignment through sequence weighting, positions-specific gap penalties and weight matrix choice. *Nucleic Acids Res* 22:4673–4680
- Tucker SL, Talbot NJ (2001) Surface attachment and pre-penetration stage development by plant pathogenic fungi. *Annu Rev Phytopathol* 39:385–417
- Vranken WF, Boucher W, Stevens TJ, Fogh RH, Pajon A, Llinas M, Ulrich EL, Markley JL, Ionides J, Laue ED (2005) The CCPN data model for NMR spectroscopy: development of a software pipeline. *Proteins* 59:687–696
- Wosten HA (2001) Hydrophobins: multipurpose proteins. *Annu Rev Microbiol* 55:625–646
- Wosten HA, de Vocht ML (2000) Hydrophobins, the fungal coat unravelled. *Biochim Biophys Acta* 1469:79–86
- Wosten HA, Asgeirsdóttir SA, Krook JH, Drenth JH, Wessels JG (1994) The fungal hydrophobin Sc3p self-assembles at the surface of aerial hyphae as a protein membrane constituting the hydrophobic rodlet layer. *Eur J Cell Biol* 63:122–129